Cell

A Hierarchical Combination of Factors Shapes the Genome-wide Topography of Yeast Meiotic Recombination Initiation

Jing Pan,[1,9,10] Mariko Sasaki,[1,5,9] Ryan Kniewel,[1,5] Hajime Murakami,[1] Hannah G. Blitzblau,[6] Sam E. Tischfield,[1,7] Xuan Zhu,[1,5] Matthew J. Neale,[1,8] Maria Jasin,[2] Nicholas D. Socci,[3] Andreas Hochwagen,[6] and Scott Keeney[1,4,*]
[1]Molecular Biology Program
[2]Developmental Biology Program
[3]Computational Biology Center
[4]Howard Hughes Medical Institute
Memorial Sloan-Kettering Cancer Center, New York, NY 10065, USA
[5]Weill Graduate School of Medical Sciences of Cornell University, New York, NY 10065, USA
[6]Whitehead Institute for Biomedical Research, Cambridge, MA 02142, USA
[7]Tri-Institutional Training Program in Computational Biology and Medicine, Cornell University, New York, NY 10065, USA
[8]Genome Damage and Stability Centre, University of Sussex, Brighton BN1 9RQ, UK
[9]These authors contributed equally to this work
[10]Present address: Cell Biology Department, University of Texas Southwestern Medical Center, Dallas, TX 75390, USA
*Correspondence: s-keeney@ski.mskcc.org
DOI 10.1016/j.cell.2011.02.009

SUMMARY

The nonrandom distribution of meiotic recombination influences patterns of inheritance and genome evolution, but chromosomal features governing this distribution are poorly understood. Formation of the DNA double-strand breaks (DSBs) that initiate recombination results in the accumulation of Spo11 protein covalently bound to small DNA fragments. By sequencing these fragments, we uncover a genome-wide DSB map of unprecedented resolution and sensitivity. We use this map to explore how DSB distribution is influenced by large-scale chromosome structures, chromatin, transcription factors, and local sequence composition. Our analysis offers mechanistic insight into DSB formation and early processing steps, supporting the view that the recombination terrain is molded by combinatorial and hierarchical interaction of factors that work on widely different size scales. This map illuminates the occurrence of DSBs in repetitive DNA elements, repair of which can lead to chromosomal rearrangements. We also discuss implications for evolutionary dynamics of recombination hot spots.

INTRODUCTION

Most sexual species induce homologous recombination in meiosis via a developmentally programmed pathway that forms numerous DNA double-strand breaks (DSBs) (Keeney, 2007). Recombination helps homologous chromosomes pair and become physically connected by crossovers, which promote accurate chromosome segregation at Meiosis I. Recombination also alters genome structure by disrupting linkage of sequence polymorphisms on the same DNA molecule (Kauppi et al., 2004). Thus, meiotic recombination is a powerful determinant of genome diversity and evolution.

Recombination is more likely to occur in some genomic regions than others, largely because of nonrandom DSB distributions (Petes, 2001; Kauppi et al., 2004). DSBs in *S. cerevisiae* show many levels of spatial organization. There are large (tens of kb) DSB hot and cold domains, within which are short regions, called hot spots, where DSBs form preferentially. Important determinants of this organization include open chromatin structure, presence of certain histone modifications, and, at some loci, binding of sequence-specific transcription factors (TFs) (Petes, 2001; Lichten, 2008). However, detailed understanding is lacking of how these and other factors influence DSB locations.

Meiotic DSBs are formed by the conserved topoisomerase-related Spo11 protein via a reaction in which a tyrosine severs the DNA backbone and attaches covalently to the 5′ end of the cleaved strand (Keeney, 2007) (Figure 1A). Two Spo11 molecules work in concert to cut both strands of a duplex. Endonucleolytic cleavage adjacent to the covalent protein-DNA complex liberates Spo11 bound to a short oligonucleotide (oligo) (Neale et al., 2005). In *S. cerevisiae* there are two major oligo subpopulations differing in length. The longer (mostly ~21–37 nt) and shorter oligos (<12 nt) are equally abundant and may reflect asymmetry of DSB processing. Further resection of 5′ DSB termini yields 3′-single stranded DNA (ssDNA) that is a substrate for strand exchange proteins.

Prior studies of genome-wide DSB distributions used either covalent Spo11-DSB complexes that accumulate in *rad50S*-like mutants or ssDNA generated by DSB resection as microarray hybridization probes (e.g., Gerton et al., 2000; Blitzblau

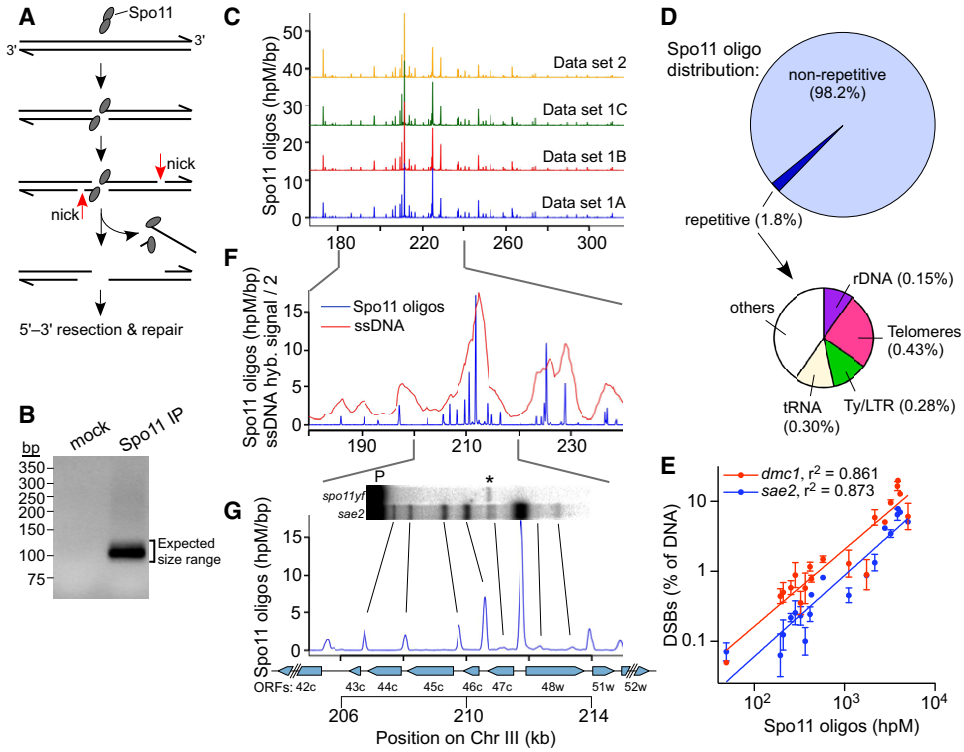

Figure 1. Mapping DSBs by Sequencing Spo11 Oligos

(A) Formation and processing of meiotic DSBs.

(B) Amplification of adaptor-ligated Spo11 oligos and mock immunoprecipitation processed in parallel.

(C) Reproducibility of Spo11 oligo maps. Oligo counts are in hpM. For the complete Spo11 oligo maps for each of the 16 chromosomes, see Figure S2.

(D) Proportions of reads mapped to unique regions and repetitive elements.

(E) Quantitative agreement of Spo11 oligos and DSBs. Oligo counts in 19 hot spots were compared with DSBs (mean ± SD, three cultures) assayed by Southern blot of DNA from *dmc1* and *sae2* mutants.

(F) The Spo11 oligo map agrees with *dmc1* ssDNA microarray analysis (Buhler et al., 2007) but has higher resolution.

(G) Agreement of the Spo11 oligo map with direct DSB detection in *sae2* genomic DNA (*spo11yf* = DSB-deficient mutant *spo11-Y135F*. P, parental band; asterisk, cross-hybridization). Oligo counts in (C), (F), and (G) were smoothed with a 201 bp sliding Hann window.

See also Figure S1 and Table S1.

et al., 2007; Buhler et al., 2007). These studies provided considerable insight but had limited quantitative and spatial resolution due to microarray design, dynamic range of hybridization signal, and the large size of DSB-associated DNA used as probes.

We overcame these limitations by using each Spo11 oligo as a tag that records precisely where a break was made. Sequencing these oligos allowed us to quantitatively map DSBs across the genome at nucleotide resolution with high sensitivity. This map elucidated chromosome features that govern DSB distributions, allowed us to test long-standing hypotheses concerning the influence of TFs, chromatin, and other factors, and uncovered mechanistic details of the formation and early nucleolytic processing of DSBs.

RESULTS AND DISCUSSION

A Nucleotide Resolution Map of Meiotic DSBs

Spo11 oligos were purified from meiotic cultures, and adaptors were added (see Figure S1A available online). Because shorter oligos are difficult to map uniquely, longer ones were enriched by size fractionation. PCR yielded products of the anticipated size that were absent in controls from mock precipitation of the meiotic extracts (Figure 1B). We deep sequenced three replicates from one culture and one from an independent culture, obtaining 2.19 million reads that were mapped to the genome of strain S288C and to a draft genome of SK1 (Liti et al., 2009), the source of Spo11 oligos (Table S1). More than 95% mapped to one or both genomes, mostly to unique sites. The maps agreed well: <0.8% of oligos mapped to different positions in the two strains (Table S1 and data not shown). The SK1 genome assembly is incomplete, so the S288C map was used for most analyses. Mapped reads matched sizes expected for longer oligos (Figure S1B). Replicates were highly reproducible (Pearson's r = 0.95–0.99) (Figure 1C and Figure S1C), so data were pooled.

Sequenced DNA was highly specific for bona fide Spo11 oligos. The rDNA cluster, 100–200 copies of a 9.1 kb repeat on Chr XII, is strongly repressed for meiotic recombination (Petes and Botstein, 1977). Only 0.15% of mappable reads were from rDNA (Figure 1D; other repeats are discussed below). Supposing

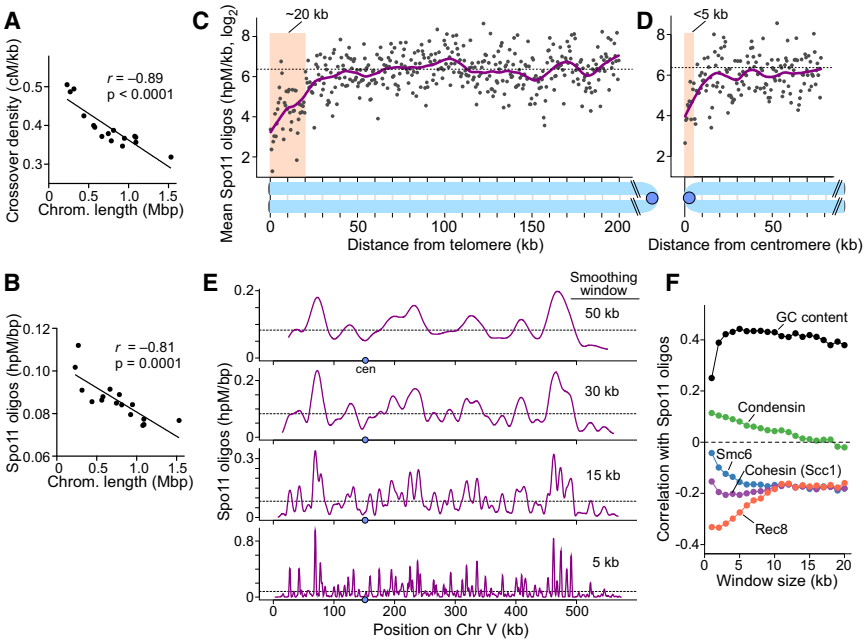

Figure 2. Large-Scale DSB Patterns

(A and B) Smaller chromosomes are hotter for crossing over (A, centimorgans [cM] per kb; data of Mancera et al., 2008) and DSBs (B).

(C and D) Telomere-proximal and pericentric DSB suppression. Points are oligo densities in 500 bp segments averaged across all 32 chromosome arms. Dashed line shows genome average, magenta line indicates smoothed fit (Lowess), and shading illustrates DSB suppression zones.

(E) Multiple levels of spatial organization of the DSB landscape. Oligo distributions on Chr V were smoothed with different-sized Hann windows. Dashed lines, genome average.

(F) Correlation (Pearson's *r*) between Spo11 oligo density and GC content or binding of chromosome structure proteins, analyzed in variable-sized windows. Rec8 data were from 2 hr in meiosis (Kugou et al., 2009); others were from vegetative cells (Lindroos et al., 2006; D'Ambrosio et al., 2008).

See also Extended Experimental Procedures and Figure S3.

that none of the rDNA reads is a true Spo11 oligo, then the Spo11-independent background is 0.0011 hits per million mapped reads (hpM) per bp (assuming 150 rDNA repeats). This is likely an overestimate because meiotic DSBs probably do form in the rDNA. Even so, this value is 75-fold below genome average (0.083 hpM/bp) and is 146- to 6646-fold below oligo densities in hot spots.

The Spo11 oligo map showed spatial and quantitative agreement with direct assays of DSBs in genomic DNA (Figures 1E and 1G), and matched or exceeded sensitivity of DSB detection from *rad50S*-like mutants (e.g., note weak signals in the *YCR048w* ORF, Figure 1G). This agreement allows us to convert oligo counts to percentage of DNA broken (Figure 1E), from which we estimate that ~160 DSBs form in nonrepetitive sequences per meiotic cell in wild-type (see Extended Experimental Procedures). This value agrees with prior estimates (Buhler et al., 2007) and can account for detectable crossovers and noncrossovers (mean = 136.7 recombination events per meiosis) (Mancera et al., 2008).

As expected from prior studies (Petes, 2001; Lichten, 2008), most Spo11 oligos were from intergenic regions containing promoters, but a significant number mapped within ORFs (Figure 1G and Figure S1D). Our oligo map agrees with microarray hybridization of ssDNA from *dmc1* mutants (Blitzblau et al., 2007; Buhler et al., 2007; Borde et al., 2009) but provides much higher resolution (Figure 1F and Figure S1E).

Thus, sequencing Spo11 oligos provides a genome-wide DSB map with unprecedented spatial and quantitative accuracy in recombination-proficient strains (Figure S2). Below, we explore this map at increasingly finer scale, from whole chromosome to single nucleotide. This analysis defines factors that interact in a hierarchical and combinatorial manner to shape DSB distributions.

Chromosome Size-Correlated Variation in DSB Frequencies

We exploited the quantitative nature of our data to address the mechanisms behind chromosome size-associated variation in recombination. Small chromosomes cross over more often per kb than longer chromosomes (Kaback et al., 1992) (Figure 2A). Previously proposed mechanisms include smaller chromosomes having higher hot spot density, having more DSBs, favoring a crossover instead of noncrossover recombination outcome, and/or having less crossover interference (Kaback et al., 1992; Gerton et al., 2000; Martini et al., 2006; Blitzblau et al., 2007).

Similar to crossovers, more Spo11 oligos per kb were recovered from smaller chromosomes (Figure 2B and Figure S3A), so crossover density correlated strongly with oligo density (r = 0.79) (Figure S3B). In contrast, there appeared to be little difference between large and small chromosomes for either the crossover versus noncrossover decision (Figure S3C), or the choice of homolog versus sister chromatid as partner for recombination (Figure S3D). We infer that smaller chromosomes tend to experience more DSBs per kb, accounting for much of the crossover density variation. Spo11 oligo hot spots (described below) occurred at similar density on all chromosomes (Figure S3E), so the greater DSB density on smaller chromosomes is not simply because of a higher density of favorable DSB sites.

Subchromosomal Domains of Suppressed or Enhanced DSB Formation

Telomere-Proximal Regions

Spo11 oligos were less frequent in the 20 kb closest to each telomere (Figure 2C), matching DSB suppression zones seen by ssDNA mapping (Blitzblau et al., 2007; Buhler et al., 2007). Telomere structures in SK1 are not well defined, but inferring

from the S288C map, oligo counts were 3.5-fold lower than genome average in the telomere-proximal 20 kb ($p < 10^{-15}$ compared to a random sample, Mann-Whitney). Although most oligos from subtelomeric repeats do not map uniquely, their aggregate contribution can be estimated. If repeats were omitted, oligo counts appeared even more reduced (6.5-fold; data not shown). Notwithstanding this suppression, 1.5% of oligos mapped within 20 kb of a telomere, suggesting that meiotic cells experience two to three such DSBs on average, consistent with crossover rates near chromosome ends (Barton et al., 2008).

Pericentric Regions

DSBs are suppressed near centromeres, but as resolution of whole-genome methods has increased, size estimates for suppressed zones have decreased from ~20 kb (Gerton et al., 2000) to ~8–10 kb (Buhler et al., 2007). In our study, strong reduction extended only a short distance compared to telomeres: Spo11 oligo density was 7-fold lower in the 3 kb surrounding centromeres compared with a randomized sample ($p < 10^{-4}$, Mann-Whitney), whereas segments further away were 2- to 3-fold lower than random but within genome-wide variation (Figure 2D and Figure S3F). We observed hot spots near centromeres in agreement with Blitzblau et al. (2007) (Table S2), but hot spot density was lower than expected within 10 kb of centromeres (60%; $p < 0.02$), and hot spot strength within 5 kb tended to be weaker (mean = 3.3-fold; $p < 0.01$) (Figures S3G and S3H). We infer that DSBs are rare within 1–3 kb of centromeres and that ~5–10 kb on either side is below average. In total, 0.4% of oligos mapped within 5 kb of centromeres, equivalent to ~0.6 DSB per meiosis. Interestingly, pericentric oligo density varied 6.5-fold between chromosomes (Figure S3I), suggesting that different chromosomes may have different propensity toward missegregation caused by recombination disrupting pericentric cohesion (Rockmill et al., 2006; Chen et al., 2008).

Interstitial Regions

Chromosomes show alternating domains of inherently higher or lower DSB frequency (Borde et al., 1999; Petes, 2001; Blat et al., 2002), which can be visualized by smoothing Spo11 oligo distributions with windows of increasing size (Figure 2E). Analyzed this way, peak spacing and peak-to-valley ratios varied substantially between regions (Figure 2E and data not shown), so the domains do not alternate in a highly regular fashion.

To explore mechanisms underlying these domains, we compared oligo distributions to several higher-order chromosome structural features. Consistent with prior studies (Gerton et al., 2000; Blat et al., 2002), Spo11 oligos correlated positively with GC content. However, additional patterns emerged when correlations were evaluated using data binned in windows of varying sizes, such that the correlation with GC content was weak over short distances (~1 kb) but was uniformly strong at longer ranges (Figure 2F). This pattern reflects superposition of at least two levels of spatial organization: DSBs occur more often in relatively GC-rich domains but at finer scale are mostly in intergenic regions (Figure S1D), which tend to be more AT rich than their surroundings.

Spo11 oligos correlated negatively with presence of meiosis-specific cohesin subunit Rec8, as expected (Kugou et al., 2009), but anticorrelation was strongest at short range (<5 kb) and was weaker at larger scales (Figure 2F). This pattern also likely reflects superposition of different levels of spatial organization. Anticorrelation in larger windows is consistent with the hypothesis that a fundamental organizing principle of DSB distributions is the arrangement of chromosomes as ~10–20 kb chromatin loops emanating from a cohesin-enriched axis, with DSBs forming preferentially in cohesin-poor loops (Blat et al., 2002; Kleckner, 2006). Why anticorrelation is even stronger at short range is unknown but may reflect a tendency for Rec8 to be especially depleted in promoters.

We also compared our data with mitotic distributions of other chromosome structure proteins (Lindroos et al., 2006; D'Ambrosio et al., 2008). Spo11 oligos showed only a weak correlation at short distances with mitotic condensin, but there was a strong anticorrelation with the G2/M distribution of Smc6 and, as previously noted, the mitotic cohesin subunit Scc1/Mcd1 (Blat and Kleckner [1999]; Figure 2F). This is consistent with the known correlation between Scc1 and the Smc5/6 complex (Lindroos et al., 2006), but the anticorrelation of Spo11 oligos with the two proteins had different size dependence.

Taken together, these patterns point to existence of multiple levels of spatial organization of the DSB terrain, supporting the view that DSB distributions are shaped by numerous high-order chromosome structures that vary over different size scales and that intersect in complex combinations (Petes, 2001; Kleckner, 2006; Keeney, 2007).

Comprehensive Identification of DSB Hot Spots

We defined 3604 DSB hot spots as clusters of Spo11 oligos (Figure 3A, Table S2, and Extended Experimental Procedures). These hot spots agreed well with direct DSB detection both spatially (e.g., Figure 1G) and quantitatively (Figure 1E), and included 94 hot spots previously documented in SK1 by Southern blot (Extended Experimental Procedures). Spo11 oligo hot spots account for nearly all hot spots identified by ssDNA mapping (Blitzblau et al., 2007; Buhler et al., 2007; Borde et al., 2009), if allowance is made for spatial ambiguity from DSB hyperresection in *dmc1* mutants (Figure 3A and Figure S4A). However, increased spatial precision of Spo11 oligo hot spot determination (Figure 3A and Figure S4A) resolved hot spots that were merged in microarray data by overlapping ssDNA resection tracts (Figure 3A). Thus, Spo11 oligos provide the highest resolution and most complete compilation of DSB hot spots available to date in a recombination-proficient organism.

Canonical and Noncanonical Characteristics of DSB Hot Spots

Apparent hot spot traits emerged from prior studies, such as a narrow width (~50–250 bp) and a tendency to overlap promoters (Petes, 2001; Lichten, 2008). However, because few hot spots have been studied in detail and previous whole-genome data do not resolve individual hot spots, the full range of variability was unknown. Spo11 oligos address this issue and reveal additional features.

Oligo hot spots had a median width of 189 bp, and 73.4% were 50–300 bp wide (Figure S4B). Most (88.2%) overlapped with promoters (Table S2), agreeing with studies of Chr III (Baudat and Nicolas, 1997). Thus, most hot spots conform to stereotypical patterns inferred from direct mapping of a small subset. Nonetheless, there were many exceptions. For example,

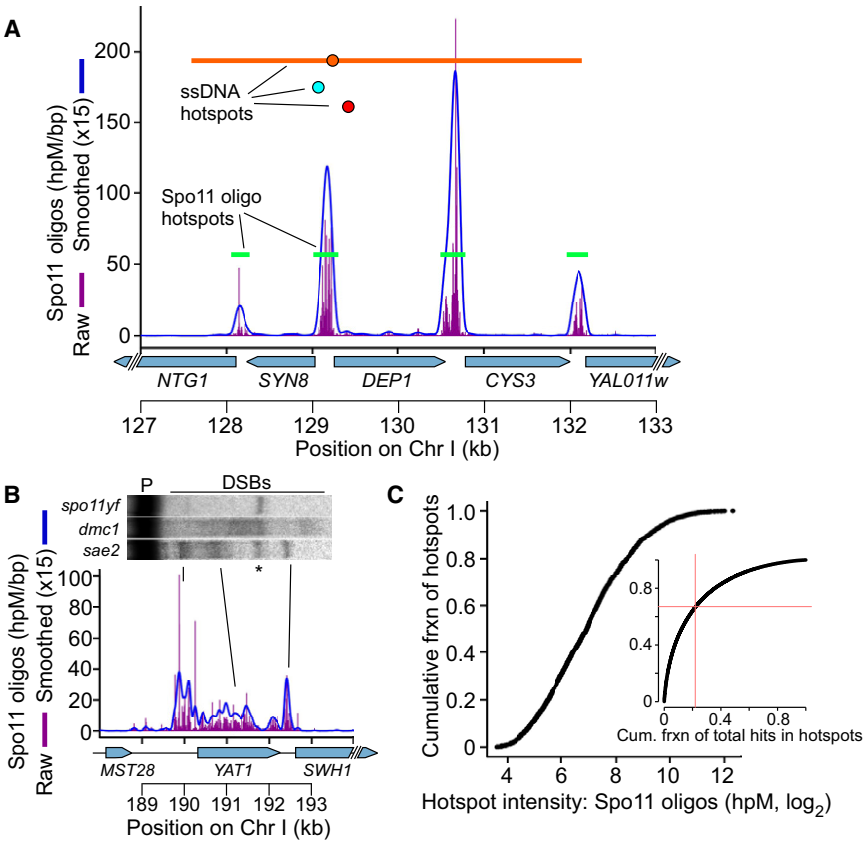

Figure 3. Identification and Properties of DSB Hot Spots

(A) Hot spots near *CYS3*. Green bars are hot spots from this study. Hot spots from ssDNA mapping are also indicated (red and teal circles, peaks only [Buhler et al., 2007; Borde et al., 2009]; orange circle and line, peak and region with signal over threshold [Blitzblau et al., 2007]).

(B) Verification of an unusually broad hot spot by Southern blot of genomic DNA (labels as in Figure 1G). DSB signal in *dmc1* spreads out because of hyperresection.

(C) Hot spot intensities vary over a smooth continuum. Inset shows cumulative fraction of hot spots versus cumulative fraction of Spo11 oligos. Red lines mark the fraction of hot spot oligos in the weakest 67% of hot spots.

For more comprehensive data for DSB hot spots, see also Figure S4 and Table S2.

10.4% of hot spots were ≥500 bp wide, and nine were >1.5 kb wide (Figure S4B). Where tested, direct assays verified anomalously wide hot spots, some of which overlapped ORFs (Figure 3B and Figure S4C; see also below). Moreover, nonpromoter hot spots accounted for 4.8% of uniquely mapped Spo11 oligos.

When hot spots were rank ordered, their oligo counts followed a smooth continuum over a 410-fold range (Figure 3C). This pattern has several implications. First, lack of an obvious break in the continuum indicates that the cutoff is arbitrary between sites that are hot spots and those that are not. Second, most hot spots were very similar to neighbors on the continuum. Thus, small changes in measured DSB activity can cause large changes in hot spot rank, which may contribute to variability of hot spot compilations that implicitly rely on rank ordering. Third, the strongest 33% of hot spots contained >75% of all hot spot-associated oligos (Figure 3C, inset). Thus, most DSBs occur in a small subset of hot spots, whereas many different sites account for a smaller (but still substantial) fraction of DSBs. Strikingly, 11% of uniquely mapped Spo11 oligos fell outside of clear hot spots. Thus, a purely hot spot-centric view misses a considerable fraction of total recombination events.

Nucleosome-Depleted Regions as Windows of Opportunity for DSB Formation

Of the few hot spots tested to date, most are nuclease-hypersensitive sites in chromatin of meiotic and vegetative cells (Petes, 2001; Lichten, 2008). Thus, an open chromatin structure is inferred to be necessary for Spo11 to access its DNA substrate, but the genome-wide relationship between DSBs and nucleosome occupancy remains unexplored. Therefore, we generated high-resolution maps of micrococcal nuclease (MNase)-resistant mononucleosomes during meiosis and compared them to Spo11 oligos.

Nucleosome occupancy was determined as previously described (Kaplan et al., 2009) (Figure S5A and Extended Experimental Procedures). Chromatin digestion and deep sequencing were carried out in two laboratories at 0, 1, 2, and 3 hr (data set N1) ,and 0 and 4 hr in meiosis (data set N2), respectively. Data set N2 samples were more heavily MNase digested, but the two data sets nonetheless agreed well for patterns described below. (See Extended Experimental Procedures and Figures S5B–S5D for additional discussion.) Relatively few differences were observed when comparing premeiotic (0 hr) with meiotic samples, indicating that steady-state nucleosome occupancy changes little during early meiosis. Moreover, patterns agreed well with prior studies in vegetatively growing haploids of different strains (Jiang and Pugh, 2009), attesting to the conserved structure of yeast chromatin (Radman-Livaja and Rando, 2010; Tsankov et al., 2010).

Most *S. cerevisiae* promoters exhibit a short (~130 bp) NDR flanked by well-positioned nucleosomes, with the transcription start site (TSS) in the first (+1) nucleosome (Radman-Livaja and Rando, 2010) (Figure 4A). Substantial overlap of DSBs with promoters is largely explained by DNA accessibility in this stereotypical structure (Lichten, 2008). As expected, Spo11 oligos mapped preferentially in promoter NDRs (Figures 4B and 4C).

Most Pol II promoters (~80%) lack a TATA sequence; this class is enriched for constitutively expressed genes, whereas TATA-containing promoters are more common for inducible

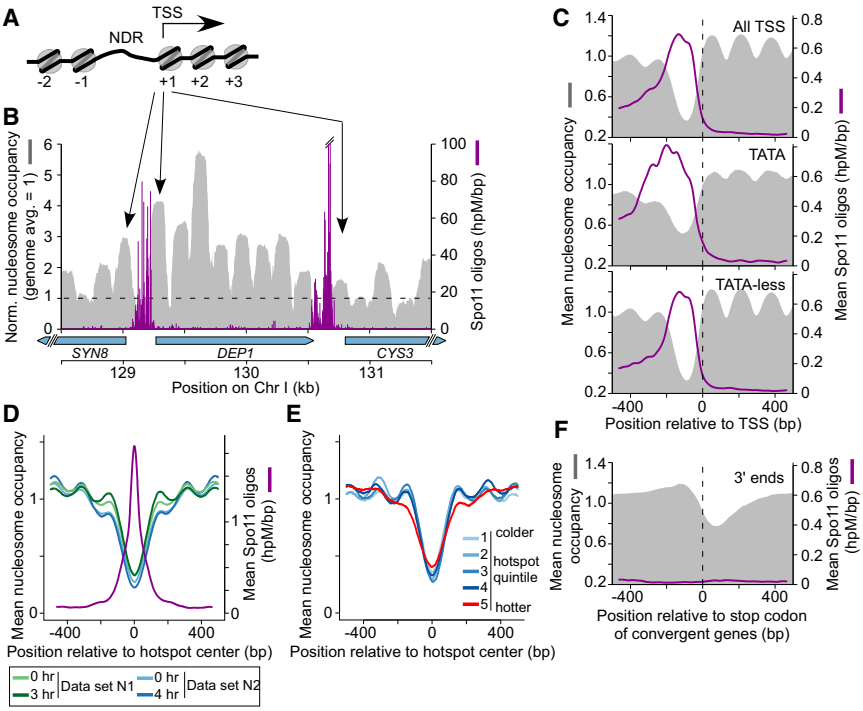

Figure 4. DSB Formation and Local Chromatin Structure

(A) Stereotypical chromatin structure of most yeast promoters.

(B) Spo11 oligos cluster in promoter NDRs. Normalized nucleosome occupancy is the number of sequence reads covering a base pair divided by genome average coverage (Kaplan et al., 2009).

(C) Genome average nucleosome occupancy and Spo11 oligo density around all annotated TSS and separately for TATA-containing and TATA-less genes.

(D) Hot spots are nucleosome depleted (n = 3600, omitting exogenous hot spots).

(E) DSB activity is not correlated with degree of nucleosome depletion at hot spot centers. Hot spots were divided into quintiles by oligo count.

(F) Low nucleosome occupancy is not sufficient for strong DSB activity. Mean profiles are shown for 3′ ends of convergent genes. Spo11 oligos in (C), (D), (F) were smoothed with a 75 bp Hann window.

For more details regarding the relationship between chromatin structure and DSB formation, see also Figure S5.

genes (Basehoar et al., 2004). These classes differed in average chromatin structure: TATA-less promoters had a narrower average NDR and well-positioned +1 and −1 nucleosomes; whereas TATA-containing promoters had a wider average NDR (Figure 4C) (Mavrich et al., 2008). Spo11 oligo distributions matched this difference (Figure 4C). TATA-containing promoters also had a 1.5-fold higher mean oligo count (Figure 4C and Figure S5E), which may account for amino acid biosynthetic genes being enriched in hot spots in a prior study (Gerton et al., 2000). TATA-containing promoters have a higher level of histone turnover, potentially providing opportunities for increased access by Spo11 (Tirosh and Barkai, 2008).

The conclusion that DSBs occur nearly exclusively on nonnucleosomal DNA is reinforced by the fact that essentially all Spo11 oligo hot spots had low nucleosome occupancy (Figure 4D and Figure S5F). However, hot spot oligo counts did not correlate with quantitative scores for nucleosome occupancy (Figure 4E). Moreover, low nucleosome occupancy is not sufficient for robust DSB formation. For example, NDRs are also prominent at 3′ ends of genes (Kaplan et al., 2009) (Figures S5D and S5G), but these are not strong DSB sites unless they coincide with the promoter NDR of a downstream gene (Figure 4F).

The hottest fifth of hot spots showed a wider average zone of low nucleosome occupancy (red line, Figure 4E). Because stronger hot spots tended to be wider on average (Figure S4B), we examined chromatin separately for "normal" width hot spots and unusually wide ones. Indeed, wider hot spots tended to have wider regions of nucleosome depletion (Figure S5H), suggesting that chromatin structure is a primary determinant of hot spot width. This conclusion is further supported by the exceptionally wide hot spots at *YAT1*, *NAR1*, and *WHI5*, where overall nucleosome occupancy was low, and nucleosomes appeared relatively disordered (Figure S4D), suggesting that stably bound nucleosomes are sparse and variably positioned among cells.

Our findings support the view that stable nucleosomes occlude Spo11 access to DNA in vivo, in turn suggesting that variability of nucleosome occupancy contributes to variation in the DSB landscape between individual cells or between strains. However, although lack of a nucleosome is a prerequisite for DSB formation, other factors play a more dominant role in determining the probability of DNA cleavage.

Influence of TFs on DSB Spatial Patterns

The effect on DSB formation of a few TFs—Bas1, Bas2, and Rap1—has been explored (reviewed in Petes, 2001). It was hypothesized that TF binding (but not transcription) promotes DSBs nearby by influencing chromatin structure and/or interacting with the DSB machinery (Petes, 2001). It was also hypothesized that TFs compete with Spo11 for DNA access, occluding DSB formation at their binding sites (Xu and Petes, 1996; Petes, 2001). Spo11 oligos allowed us to test these hypotheses genome wide.

Spo11 oligos mapped frequently near 4233 binding sites of 77 TFs annotated based on chromatin immunoprecipitation and conservation (MacIsaac et al., 2006) (Figures 5A and 5B), which is not surprising because TF sites are enriched in promoters. We examined fine-scale patterns by grouping TFs based on local oligo distributions (Figure 5C and Table S3). We discuss three of these groups below. Other TFs are not considered further because they showed little spatial correlation with Spo11 oligos,

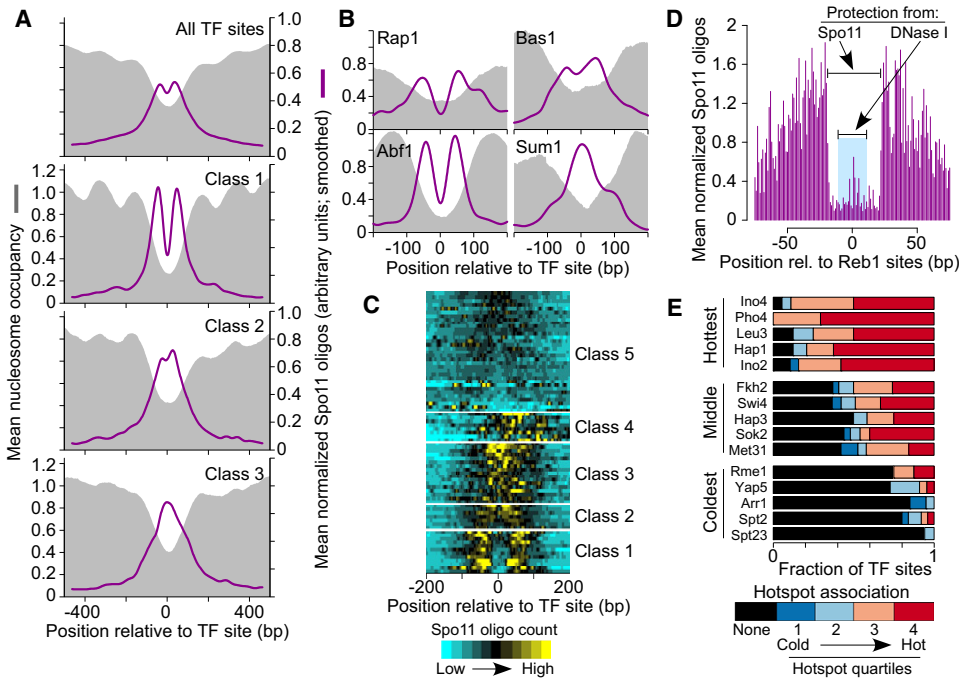

Figure 5. DSB Patterns around TF Binding Sites

(A and B) Mean normalized Spo11 oligo profiles (see Extended Experimental Procedures), smoothed with a 75 bp window, and nucleosome occupancy (3-hr sample) around TF sites.

(C) TFs clustered according to local spatial pattern of Spo11 oligos. Each horizontal line on the heat map shows the mean profile for binding sites of a single TF, grouped by k-means clustering. Because locally normalized oligo counts were used, color coding reflects DSB spatial pattern, not total DSB intensity.

(D) Zones of protection from Spo11 or DNase I (Hesselberth et al., 2009) around Reb1-binding sites (n = 156).

(E) TFs that are most or least associated with frequent DSB formation nearby. TFs were rank ordered by mean oligo count ±500 bp from their binding sites. A subset of TFs is shown; others are in Figure S6B. Bars depict the fraction of sites not in hot spots (black) and divide the remainder according to hot spot quartile. For further information about the relationship between TFs and DSB formation, see Figure S6 and Table S3.

having either local oligo enrichment offset from the TF sites (Class 4 in Figure 5C) or evenly distributed oligos (Class 5).

For 12 TFs, there was strong evidence for DSB occlusion at their binding sites (Class 1, Figures 5A and 5C). The two most striking examples were Abf1 and Reb1, whose binding sites were often located in Spo11 oligo hot spots (Table S3). Both proteins showed strong oligo enrichment adjacent to their sites but depletion in the central ~40 bp (Figures 5B and 5D and Figure S6A). Abf1 or Reb1 binding promotes nucleosome exclusion nearby (Badis et al., 2008; Kaplan et al., 2009), and both bind chromatin in meiosis (Schlecht et al., 2008), so it is likely that they influence hot spot activity at least indirectly by providing favorable chromatin structure. Class 1 also includes Rap1 (Figure 5B and Figure S6A), whose binding sites occluded DSB formation in an altered *HIS4* hot spot (Xu and Petes, 1996). Our results show that Spo11 tends to be prevented from cutting in natural Rap1-binding sites genome wide.

Abf1, Reb1, and Rap1 footprints of protection against Spo11 cleavage (40–42 bp) were larger than for protection from DNase I cleavage in chromatin (19–24 bp) (Hesselberth et al., 2009) (Figure 5D and Figure S6A). We infer that Spo11 (and associated proteins) has a larger effective size than DNase I for cleaving DNA and that steric constraints place the Spo11 active site ≥10 bp (30–40 Å) away from surfaces of competing DNA-binding proteins. The findings also suggest that it is unlikely that Spo11-associated proteins must form an extensive DNA-binding surface prior to DNA binding by Spo11 itself.

Seven TFs showed only weak DSB occlusion at their binding sites (Class 2, Figures 5A and 5C). A good example is Bas1. Consistent with prior studies (Mieczkowski et al., 2006), 32/37 (86.5%) analyzed Bas1 sites were in 18 Spo11 oligo hot spots (Table S3). However, Bas1 sites showed only modest depression of oligo counts in their immediate vicinity (Figure 5B). Thus, not all TFs that affect DSBs can block Spo11 access to DNA. Class 2 TFs may have low steady-state occupancy of their binding sites when DSBs form (e.g., because of short dwell time on DNA, or because they act earlier), or Spo11 and/or accessory factors can displace them.

Binding sites for another 17 TFs showed local oligo enrichment, but, unlike Classes 1 or 2, no detectable DSB occlusion (Class 3, Figures 5A and 5C). An example is Sum1 (Figure 5B), which represses meiotic genes in vegetative cells and is displaced during meiosis (Ahmed et al., 2009). Thus, some Class 3 TFs may not block Spo11 simply because they are not chromatin bound at the relevant time. Nevertheless, some may influence DSBs by prior hit-and-run action on nucleosome occupancy or histone modifications.

Correlating TF-Binding Sites with DSB Frequency

We also examined whether TFs can be linked, positively or negatively, to DSB hot spot activity. TFs differed widely when we compared the average total oligo counts near their binding sites (Figure 5E and Figure S6B). TF classes defined above did not correlate with oligo counts (Figure S6C); thus, DSB frequency and DSB spatial distribution are separate features of the interplay between TFs and DSBs. The five TFs with the highest mean oligo counts (the Ino2/Ino4 complex, Pho4, Leu3, and Hap1; Figure 5E) are not known to influence meiotic recombination, but enrichment of Pho4 sites in hot spots was noted before (Gerton et al., 2000). It is not yet clear whether these TFs are active players or innocent bystanders in hot spot activity, but their known properties are consistent with their being bound to target promoters during sporulation (Figure S6 legend). On the other end of the scale, several TFs had low oligo counts near their binding sites (Figure 5E). Most have not been characterized in meiosis, but it may be that they do not exist in SK1 (Figure S6 legend), are not expressed or not bound to targets during meiosis, or are linked to formation of closed chromatin that inhibits DSBs.

Thus, these findings reveal TFs whose binding sites are predictive of hot spot activity or lack thereof. However, for most TFs, oligo counts varied widely between individual binding sites. For example, Fkh2 and Swi4 sites were about equally likely to be in a hot spot as not, and the hot spots they were associated with ran the gamut from weak to strong (Figure 5E). Most TFs had similar characteristics (Figure 5E and Figure S6B), so presence of these binding sites is a poor predictor of DSB frequency. This pattern reinforces the view that promoters provide windows of opportunity for Spo11, but DSB frequency is more strongly dictated by other factors.

Fine-Scale Analysis of DSB Sites

Spo11 displays biases for which phosphodiester bonds are cleaved, but it has been difficult to discern the patterns behind these preferences (Keeney, 2007; Murakami and Nicolas, 2009). Our data now provide a large library of individual cleavage sites, with the fine-scale Spo11 oligo distribution agreeing with direct DSB mapping ($r = 0.77$; Figure S7A) (Murakami and Nicolas, 2009), after accounting for spatial ambiguity of oligos whose 5′ ends map next to C residues (Figure S1A).

To explore Spo11 preferences, we aligned DNA sequences around each uniquely mapped oligo, using the SK1 genome sequence (Figure 6A and Figure S7B). All mapped oligos were included, but conclusions discussed below were also obtained if we used only oligos without 5′-C ambiguity (data not shown). No consensus was apparent, supporting the idea that Spo11 is flexible in terms of DNA sequences it can cleave (Murakami and Nicolas, 2009). Nonetheless, base composition was highly nonrandom from −16 to +30 relative to the predicted dyad axis of cleavage (Figure S7B). Figure 6B summarizes this pattern. The strongest bias encompassed 10–12 bp centered on the dyad axis (segment "a," Figure 6B), a region predicted to contact Spo11 based on docking DNA against Top6A, the archaeal Spo11 homolog (Nichols et al., 1999) (Figure 6C). This biased composition likely reflects DNA properties promoting Spo11 binding and/or catalysis, so we examined this region in detail. Overall, it is AT enriched (64.6% versus 60.3% local average), and the dinucleotide composition is consistent with a preference for relatively narrow, deep grooves on the side of the DNA facing Spo11 (Figure S7D). G was enriched, and C was depleted at the third base in Spo11 oligos (Figure S7B), which is the complement of the base 5′ of the scissile phosphate on the opposite strand (Figure 6D). Thus, Spo11 cleavage is favored 3′ of C, and as previously shown (Murakami and Nicolas, 2009), cleavage 3′ of G is disfavored. Dinucleotide frequencies further refined Spo11 preference at the scissile phosphate: 5′-C[A/C/T] and TA were favored, whereas G[A/C/T] and AA were disfavored (Figure 6D).

Bias was also observed at 11–16 bp symmetrically to the right and left of the dyad axis, outside the predicted Spo11 footprint ("b" segments, Figures 6B and 6C). These zones, which are modestly GC enriched (41.8% versus 39.7% local average), likely reflect preference of a Spo11-associated protein or a Spo11 domain not modeled by the Top6A structure. Another region that was asymmetric relative to the dyad axis (segment "c," Figures 6B and 6C) probably reflects bias for oligo 3′-end formation, discussed below.

For the central 32 bp, dinucleotide composition on the right correlated with the reverse complementary composition on the left (Figures S7E and S7F), as predicted for 2-fold rotational symmetry around the theoretical dyad axis. This symmetry does not imply that individual Spo11 cleavage sites are palindromic. Instead, it appears that left and right half-sites contribute separately because sites with a favored base composition on one side were less likely to show favored composition on the other side (data not shown). Importantly, DNA 5′ of each oligo was engaged by Spo11 and accessory factors in vivo but was never encountered by enzymes used in vitro to manipulate the oligos. Thus, left:right symmetry demonstrates that observed biases are inherent to DSB formation and cannot be artifacts of methods to sequence Spo11 oligos.

Formation of Spo11 Oligo 3′ Ends

Because reads on the 454 platform are relatively long, we could define the 3′ end of each oligo, which is likely formed by nuclease activity of Mre11, or possibly Sae2 (Figure 6A) (Keeney, 2007). Base composition around 3′ ends was nonrandom in a pattern distinct from 5′ ends (Figure 6E and Figure S7C). Strong bias was limited to 3–4 bp centered on the 3′ ends, most notably a small but significant enrichment for T. Thus, Mre11 (or Sae2) activity appears to be only modestly affected by DNA composition around the scissile phosphate, with a slight preference for homopolymeric T runs.

Unlike 5′ ends, 3′ ends frequently mapped within boundaries of positioned nucleosomes and in TF-binding sites where 5′ ends were rare (Figures 6F and 6G and Figure S6A). Thus, neither nucleosomes nor the TFs that block Spo11 appear to be a barrier to endonucleolytic DSB processing. Possibly, Mre11-dependent cleavage can occur on DNA still bound by histones or TFs, but it seems more likely that these protein-DNA interactions are disrupted before cleavage, either through normal dynamics of histone- or TF-DNA interactions or via active displacement by Spo11 and/or accessory proteins. In principle, disruption of these protein-DNA interactions could occur either prior to or as a consequence of DSB formation. However, Mre11 associates with DSB sites independent of DSB formation (Borde

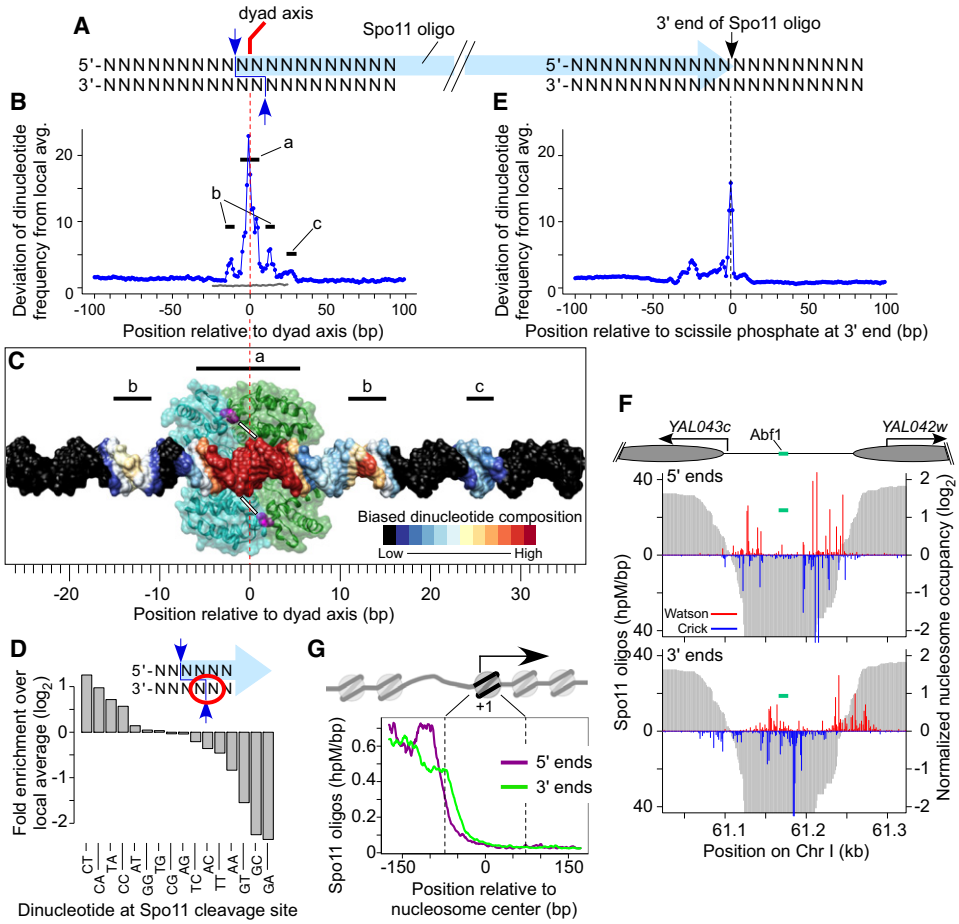

Figure 6. High-Resolution View of DSB Sites

(A) Schematic of a Spo11 DSB. Staggered cuts (blue arrows) by a Spo11 dimer generate a 2 nt 5′ overhang, the middle of which is a 2-fold rotational symmetry axis. Nucleolytic cleavage (black arrow) forms the oligo 3′ end.

(B) Nonrandom dinucleotide composition around Spo11 cleavage sites. At each position, deviation of dinucleotide frequencies from local average was summed (Extended Experimental Procedures). Gray line indicates deviation for a randomized sample of 50-mers.

(C) Biased DNA composition relative to predicted Spo11 binding. Dimeric structure is shown of a fragment of a Spo11 homolog, archaeal Top6A (Nichols et al., 1999), with monomers in green and blue, and catalytic tyrosines in magenta. White bars indicate scissile phosphates in DNA docked on the dimer and color coded by composition bias in (B).

(D) Spo11 preference at the scissile phosphate (dinucleotide indicated by the red circle).

(E) Nonrandom dinucleotide composition around 3′ ends, as in (B).

(F and G) Nucleosomes and TFs are not a barrier to 3′-end formation. (F) Spo11 oligos in an intergenic region. Cartoon depicts annotated nucleosomes (ellipses), TSS (arrows), and Abf1-binding site. Graphs show 5′ and 3′ ends of oligos from top (red) and bottom (blue) strands. Nucleosome occupancy (3 hr) is in gray. (G) Oligos around +1 nucleosomes (n = 5036). Genome averages were smoothed with 5 bp sliding window.

Figure S7 provides nucleotide resolution analysis of many DSB sites.

et al., 2004), and is required for DSBs (Keeney, 2007). Thus, we propose that assembly of Spo11-containing pre-DSB complexes on DNA competitively replaces or actively displaces other proteins. This scenario can explain increased MNase sensitivity observed in hot spots prior to DSBs (Ohta et al., 1994), much of which is in NDRs themselves and is not accompanied by loss of positioned nucleosomes (Lichten, 2008).

Evidence for Asymmetry in an Early DSB Processing Step

We proposed three models to explain the 1:1 ratio of prominent oligo subpopulations (Neale et al., 2005): each DSB could be processed asymmetrically to yield one short and one long oligo (Figure 7Aa); each DSB could be processed symmetrically to yield two long or two short oligos, with the two outcomes equally likely genome wide (Figure 7Ab); or nucleolytic cleavage could occur either near or far from each DSB, with independent positions on the left and right, and an ~50% chance for near versus far (Figure 7Ac). The latter model predicts a mix of DSBs with oligos that are asymmetric, symmetric long, or symmetric short.

Because we recovered mostly the longer oligos, symmetry can be evaluated by asking whether oligos were recovered equally from the top (“Watson”) and bottom (“Crick”) strands

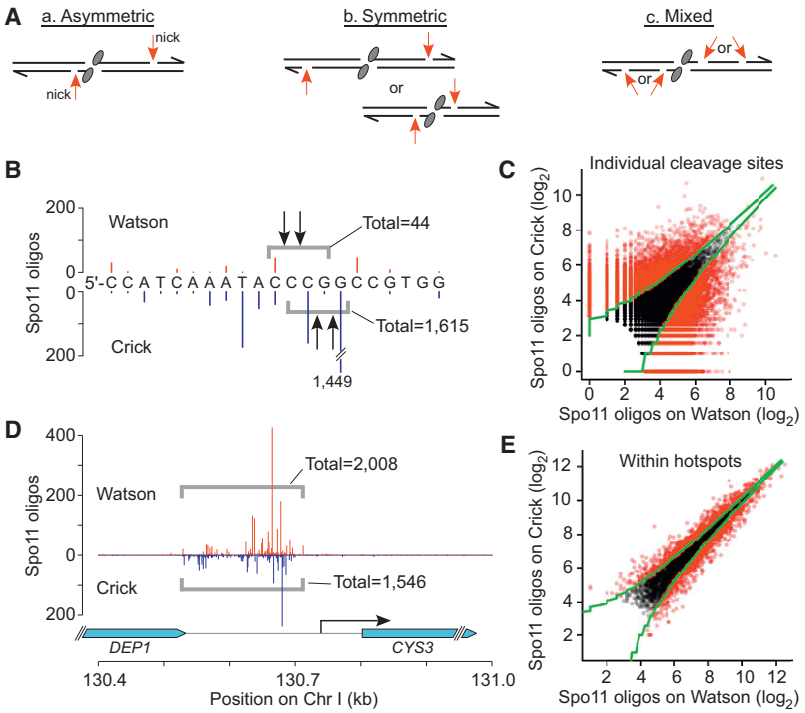

Figure 7. Spo11 Oligo Asymmetry

(A) Models for origin of long and short oligos. (a). Nicks (red arrows) positioned asymmetrically relative to Spo11. (b). Two DSB classes with symmetric nicks. (c) Variable nick placement, independent on left and right.

(B) Asymmetry at DSB sites in the *YCR048w* hot spot (Chr III, 211,744–211,764 bp). Arrows show two known DSB sites that cannot be resolved due to ambiguity of oligos with 5′-C. Gray brackets indicate regions pooled to tally oligos for each strand.

(C) Substantial asymmetry at Spo11 cleavage sites genome wide. Strand-specific counts were tallied for sites with eight or more oligos total (n = 49,115). Points in red are significantly asymmetric (Poisson test, $p \leq 0.05$ after correction for false discovery). Green lines show 95% confidence intervals for Poisson sampling with equal frequencies on Watson and Crick.

(D) Net asymmetry in the *CYS3* hot spot.

(E) Net asymmetry of hot spots genome wide (n = 3604, colors as in C).

at individual DSB positions. Figure 7B shows two strong cleavage sites in the *YCR048w* hot spot (Murakami and Nicolas, 2009). These sites are not resolved in our study because of 5′-C ambiguity, but total oligos from these sites can be tallied for the two strands (gray brackets, Figure 7B). We recovered 1615 Crick oligos, but only 44 Watson oligos, revealing strong asymmetry ($p < 2.2 \times 10^{-16}$, Poisson test). We infer that equal oligo numbers were formed on both strands in vivo but that Watson oligos often escaped detection, perhaps because they were too short.

Many DSB sites analyzed showed significant asymmetry (39.3%, Figure 7C), which is incompatible with the obligate symmetry model (Figure 7Ab) and with versions of the mixed model (Figure 7Ac) in which 3′-end positions are random every time a DSB is made. Instead, our findings are compatible with the obligate asymmetry model (Figure 7Aa). Oligo counts are a population average; thus, the fact that not all DSB sites showed asymmetry could mean that every DSB is processed asymmetrically, with different sites showing greater or lesser propensity for the direction to be the same in different cells. The results are also compatible with the mixed cleavage model (Figure 7Ac) if degree of asymmetry is particular to individual DSB sites rather than being the same genome wide.

We also evaluated hot spot asymmetry. On a population basis, asymmetric DSBs in a hot spot can either reinforce or cancel one another. For example the *CYS3* hot spot had net 1.3-fold asymmetry in favor of Watson ($p < 10^{-14}$) (Figure 7D). Of the 3604 hot spots identified, 1754 (48.7%) showed net asymmetry (Figure 7E). Direction or presence of asymmetry does not correlate with orientation of adjacent transcription units (data not shown). It remains to be determined whether hot spot asymmetry is simply the aggregate of independent DSB sites, or if directionality is influenced by as yet unknown local chromosomal features. Nonetheless, the findings provide candidate sites to test the proposal that DSB asymmetry might influence later recombination steps, such as which end is first to invade the unbroken homolog (Neale et al., 2005).

DSBs at Risk for Genome Rearrangements

DSBs in repetitive DNA can lead to genome rearrangement if nonallelic homologous sequences are used as recombination templates (reviewed in Sasaki et al., 2010). Our data allowed us to examine these "at-risk" DSBs. Only 1.53% of Spo11 oligos mapped to two or more positions in the genome, and an additional 0.23% mapped to unique positions within boundaries of repetitive elements (Figure 1D). High copy number repeats (rDNA, telomeres, retrotransposons, and tRNA genes) accounted for only 1.16% of total oligos, despite these repeats occupying ~14% of the genome. Remaining oligos that mapped to multiple locations were from low copy repeats such as multigene families or from regions with low sequence complexity. As noted above, few oligos were from rDNA; these mapped fairly uniformly across the repeat unit (Figure S1F).

Subtelomeric X and Y′ elements accounted for 0.43% of mappable reads, or ~0.7 DSBs per meiosis assuming all recovered sequences were from bona fide Spo11 oligos (Figure 1D). Most of these oligos were from Y′ elements (Figure S1F), consistent with frequent rearrangement of chromosome ends through Y′ recombination in meiosis (Horowitz et al., 1984).

S288C has 50 full Ty retrotransposons and many more solo long terminal repeats (LTRs) or LTR fragments, totaling ~3% of its genome, but SK1 has only approximately half as many full-length Tys, and insertion sites are not conserved (Gabriel et al., 2006; Liti et al., 2009) (unpublished data). Meiotic recombination was rare in artificial Ty constructs, and meiotic DSBs were not

detected in a full Ty element, likely reflecting its relatively closed chromatin structure (Ben-Aroya et al., 2004). Correspondingly, only 0.28% of Spo11 oligos were from full Tys or LTRs (Figure 1D and Figure S1F), indicating that meiotic DSBs tend to be somewhat suppressed in natural Ty elements.

These findings demonstrate that DSB formation is suppressed within repetitive DNA genome wide, albeit to various degrees for different repeat families. Nonetheless, the total burden of such DSBs is substantial: from the number of Spo11 oligos recovered, we estimate an average of approximately two to three DSBs per meiosis. Not all types of repeats have the same potential to generate lethal chromosome rearrangements through nonallelic homologous recombination, but all have potential to contribute to genome plasticity and evolution, and all have potential to adversely affect meiotic chromosome pairing and disjunction. Thus, as yet poorly understood mechanisms that control nonallelic recombination are clearly critical in nearly every meiosis to maintain genome integrity (Sasaki et al., 2010).

Conclusions

Our findings reinforce the view that the DSB landscape in *S. cerevisiae* is shaped by combinatorial action of many factors (Petes, 2001; Kleckner, 2006; Keeney, 2007; Lichten, 2008). These factors operate over many size scales and include whole chromosome variation, large subchromosomal domains, chromosome structure proteins, chromatin structure (including nucleosomes and sequence-specific DNA-binding proteins), and local DNA composition. Moreover, these factors work hierarchically, with the general trend that level in hierarchy is proportional to scale. Thus, for example, two DNA segments that are equally free of nucleosomes may have substantially different DSB probability depending on their locations relative to loop-axis chromosome organization or telomeres.

These studies also lead to reexamination of the definition of DSB hot spots. From the earliest proposals that recombination initiates preferentially at defined sites (Holliday, 1964), the concept of hot spots has been useful for describing how recombination is distributed and for cataloging preferred sites. However, we suggest that this concept also tends to lead, intentionally or not, to the view that hot spots are discrete functional entities. We show here that many base pairs—and maybe all—are potential DSB sites, with a continuous distribution of cleavage probability. We also show that hot spot definition is arbitrary, i.e., that it is difficult to draw a biologically meaningful boundary between what is and what is not a hot spot. Moreover, whereas most hot spots comprise a narrow cluster of DSB sites within a promoter, many do not fit this stereotype, and many DSBs occur outside of hot spots entirely. These findings argue against a granular, hot spot-centric view of DSB distributions. Instead, the DSB landscape is better seen as a quantitative, probabilistic distribution across the entire genome. A hot spot is a group of phosphodiester bonds that share a high local likelihood of cleavage, i.e., simply one spatial organization level among many. In this view, Spo11 is an opportunistic cutter, and hot spots are its windows of opportunity (Lichten, 2008).

As shown here and in prior studies, chromatin structure is a key determinant of these windows. Low nucleosome occupancy in promoters is conserved in *S. cerevisiae* strains and related species (this work and Tsankov et al. [2010]), likely because of selection to maintain appropriate chromatin structure for gene expression. In fact, chromosome structures at all size scales are probably under evolutionary constraints because of functions important for DNA replication, compaction, and segregation. Hence, many factors that govern Spo11 activity are under selective pressures independent of meiosis or recombination per se (Nicolas et al., 1989). This predicts that some features of DSB landscapes will show significant similarity between related yeast species: quantitative values are likely to differ substantially, but many hot spots in one strain or species are likely to be hot spots in another. In this regard, *S. cerevisiae* and its relatives may contrast with mammals, where a meiosis-specific factor, PRDM9, appears to specifically target SPO11 to sites that may not have another intrinsic function (Neale, 2010), and which might thus be easier to evolve toward hot spot extinction because of different selective constraints. It will be interesting to compare Spo11 oligo maps between species, such as mammals and budding and fission yeasts, whose chromosomes have distinct architectures and evolutionary dynamics.

EXPERIMENTAL PROCEDURES

Detailed methods are in Extended Experimental Procedures. Strains are diploid derivatives of SK1 (Table S4). The Spo11-HA construct used here gives reduced DSBs (~80% of wild-type) but does not appear to grossly alter DSB distributions (Figure S7). Spo11 oligos were sequenced as follows (Figure S1A). Cultures were harvested at 4 hr of synchronous meiosis, then denaturing extracts were prepared from nuclei of hypotonically lysed spheroplasts. Spo11-HA-oligo complexes were immunoprecipitated, size fractionated by SDS-PAGE, then protease digested. The 3′ ends of resulting Spo11 oligos were extended with GTP and terminal deoxynucleotidyl transferase, then ligated to a double-stranded DNA adaptor using T4 RNA ligase 2. The complementary strands of Spo11 oligos were synthesized, then gel purified on denaturing PAGE, and subjected to another round of 3′-GTP tailing, adaptor ligation, and strand synthesis. Sequencing primers were added by low-cycle numbers of PCR, products were sequenced on the 454 platform (Roche) according to manufacturer's instructions, and reads were mapped to S288C and SK1 genomes. Nucleosome mapping was carried out by deep sequencing of MNase-digested chromatin according to an established method (Kaplan et al., 2009). Data analysis utilized R (http://www.r-project.org/) and Bioconductor (http://www.bioconductor.org/). Map files in several formats are available for download (see Table S5 and Data S1).

ACCESSION NUMBERS

Raw sequence data are available from the GEO repository (accession numbers GSE26449 and GSE26452).

SUPPLEMENTAL INFORMATION

Supplemental Information includes Extended Experimental Procedures, seven figures, five tables, and one data file and can be found with this article online at doi:10.1016/j.cell.2011.02.009.

ACKNOWLEDGMENTS

We thank A. Viale (MSKCC Genomics Core Laboratory) for sequencing; S. Shuman and J. Nandakumar (MSKCC) for generous gifts of RNA ligase; and M. Lichten (NCI), I. Whitehouse (MSKCC), and G. Smith (Fred Hutchinson Cancer Research Center) for comments on the manuscript. This work was supported in part by NIH grants GM58673 (S.K.) and HD53855 (S.K. and

M.J.). M.J.N. is supported by a Royal Society University Research Fellowship, an MRC New Investigator Grant, and an HFSP Career Development Award. J.P. was supported by a Leukemia and Lymphoma Society Fellowship. R.K. was supported by NIH training grant T32 GM008539. S.K. is an Investigator of the Howard Hughes Medical Institute.

Received: December 3, 2010
Revised: January 13, 2011
Accepted: February 3, 2011
Published: March 3, 2011

REFERENCES

Ahmed, N.T., Bungard, D., Shin, M.E., Moore, M., and Winter, E. (2009). The Ime2 protein kinase enhances the disassociation of the Sum1 repressor from middle meiotic promoters. Mol. Cell. Biol. *29*, 4352–4362.

Badis, G., Chan, E.T., van Bakel, H., Pena-Castillo, L., Tillo, D., Tsui, K., Carlson, C.D., Gossett, A.J., Hasinoff, M.J., Warren, C.L., et al. (2008). A library of yeast transcription factor motifs reveals a widespread function for Rsc3 in targeting nucleosome exclusion at promoters. Mol. Cell *32*, 878–887.

Barton, A.B., Pekosz, M.R., Kurvathi, R.S., and Kaback, D.B. (2008). Meiotic recombination at the ends of chromosomes in *Saccharomyces cerevisiae*. Genetics *179*, 1221–1235.

Basehoar, A.D., Zanton, S.J., and Pugh, B.F. (2004). Identification and distinct regulation of yeast TATA box-containing genes. Cell *116*, 699–709.

Baudat, F., and Nicolas, A. (1997). Clustering of meiotic double-strand breaks on yeast Chromosome III. Proc. Natl. Acad. Sci. USA *94*, 5213–5218.

Ben-Aroya, S., Mieczkowski, P.A., Petes, T.D., and Kupiec, M. (2004). The compact chromatin structure of a Ty repeated sequence suppresses recombination hot spot activity in *Saccharomyces cerevisiae*. Mol. Cell *15*, 221–231.

Blat, Y., and Kleckner, N. (1999). Cohesins bind to preferential sites along yeast chromosome III, with differential regulation along arms versus the centric region. Cell *98*, 249–259.

Blat, Y., Protacio, R.U., Hunter, N., and Kleckner, N. (2002). Physical and functional interactions among basic chromosome organizational features govern early steps of meiotic chiasma formation. Cell *111*, 791–802.

Blitzblau, H.G., Bell, G.W., Rodriguez, J., Bell, S.P., and Hochwagen, A. (2007). Mapping of meiotic single-stranded DNA reveals double-strand-break hot spots near centromeres and telomeres. Curr. Biol. *17*, 2003–2012.

Borde, V., Wu, T.-C., and Lichten, M. (1999). Use of a recombination reporter insert to define meiotic recombination domains on Chromosome III of *Saccharomyces cerevisiae*. Mol. Cell. Biol. *19*, 4832–4842.

Borde, V., Lin, W., Novikov, E., Petrini, J.H., Lichten, M., and Nicolas, A. (2004). Association of Mre11p with double-strand break sites during yeast meiosis. Mol. Cell *13*, 389–401.

Borde, V., Robine, N., Lin, W., Bonfils, S., Geli, V., and Nicolas, A. (2009). Histone H3 lysine 4 trimethylation marks meiotic recombination initiation sites. EMBO J. *28*, 99–111.

Buhler, C., Borde, V., and Lichten, M. (2007). Mapping meiotic single-strand DNA reveals a new landscape of DNA double-strand breaks in *Saccharomyces cerevisiae*. PLoS Biol. *5*, e324.

Chen, S.Y., Tsubouchi, T., Rockmill, B., Sandler, J.S., Richards, D.R., Vader, G., Hochwagen, A., Roeder, G.S., and Fung, J.C. (2008). Global analysis of the meiotic crossover landscape. Dev. Cell *15*, 401–415.

D'Ambrosio, C., Schmidt, C.K., Katou, Y., Kelly, G., Itoh, T., Shirahige, K., and Uhlmann, F. (2008). Identification of cis-acting sites for condensin loading onto budding yeast chromosomes. Genes Dev. *22*, 2215–2227.

Gabriel, A., Dapprich, J., Kunkel, M., Gresham, D., Pratt, S.C., and Dunham, M.J. (2006). Global mapping of transposon location. PLoS Genet. *2*, e212.

Gerton, J.L., DeRisi, J., Shroff, R., Lichten, M., Brown, P.O., and Petes, T.D. (2000). Inaugural article: global mapping of meiotic recombination hot spots and coldspots in the yeast *Saccharomyces cerevisiae*. Proc. Natl. Acad. Sci. USA *97*, 11383–11390.

Hesselberth, J.R., Chen, X., Zhang, Z., Sabo, P.J., Sandstrom, R., Reynolds, A.P., Thurman, R.E., Neph, S., Kuehn, M.S., Noble, W.S., et al. (2009). Global mapping of protein-DNA interactions in vivo by digital genomic footprinting. Nat. Methods *6*, 283–289.

Holliday, R. (1964). A mechanism for gene conversion in fungi. Genet. Res. *5*, 282–304.

Horowitz, H., Thorburn, P., and Haber, J.E. (1984). Rearrangements of highly polymorphic regions near telomeres of *Saccharomyces cerevisiae*. Mol. Cell. Biol. *4*, 2509–2517.

Jiang, C., and Pugh, B.F. (2009). A compiled and systematic reference map of nucleosome positions across the *Saccharomyces cerevisiae* genome. Genome Biol. *10*, R109.

Kaback, D.B., Guacci, V., Barber, D., and Mahon, J.W. (1992). Chromosome size-dependent control of meiotic recombination. Science *256*, 228–232.

Kaplan, N., Moore, I.K., Fondufe-Mittendorf, Y., Gossett, A.J., Tillo, D., Field, Y., LeProust, E.M., Hughes, T.R., Lieb, J.D., Widom, J., et al. (2009). The DNA-encoded nucleosome organization of a eukaryotic genome. Nature *458*, 362–366.

Kauppi, L., Jeffreys, A.J., and Keeney, S. (2004). Where the crossovers are: recombination distributions in mammals. Nat. Rev. Genet. *5*, 413–424.

Keeney, S. (2007). Spo11 and the formation of DNA double-strand breaks in meiosis. In Recombination and Meiosis, D.H. Lankenau, ed. (Heidelberg, Germany: Springer-Verlag), pp. 81–123.

Kleckner, N. (2006). Chiasma formation: chromatin/axis interplay and the role (s) of the synaptonemal complex. Chromosoma *115*, 175–194.

Kugou, K., Fukuda, T., Yamada, S., Ito, M., Sasanuma, H., Mori, S., Katou, Y., Itoh, T., Matsumoto, K., Shibata, T., et al. (2009). Rec8 guides canonical Spo11 distribution along yeast meiotic chromosomes. Mol. Biol. Cell *20*, 3064–3076.

Lichten, M. (2008). Meiotic chromatin: the substrate for recombination initiation. In Recombination and Meiosis: Models, Means, and Evolution, R. Egel and D.H. Lankenau, eds. (Berlin: Springer-Verlag), pp. 165–193.

Lindroos, H.B., Strom, L., Itoh, T., Katou, Y., Shirahige, K., and Sjogren, C. (2006). Chromosomal association of the Smc5/6 complex reveals that it functions in differently regulated pathways. Mol. Cell *22*, 755–767.

Liti, G., Carter, D.M., Moses, A.M., Warringer, J., Parts, L., James, S.A., Davey, R.P., Roberts, I.N., Burt, A., Koufopanou, V., et al. (2009). Population genomics of domestic and wild yeasts. Nature *458*, 337–341.

MacIsaac, K.D., Wang, T., Gordon, D.B., Gifford, D.K., Stormo, G.D., and Fraenkel, E. (2006). An improved map of conserved regulatory sites for *Saccharomyces cerevisiae*. BMC Bioinformatics *7*, 113.

Mancera, E., Bourgon, R., Brozzi, A., Huber, W., and Steinmetz, L.M. (2008). High-resolution mapping of meiotic crossovers and non-crossovers in yeast. Nature *454*, 479–485.

Martini, E., Diaz, R.L., Hunter, N., and Keeney, S. (2006). Crossover homeostasis in yeast meiosis. Cell *126*, 285–295.

Mavrich, T.N., Ioshikhes, I.P., Venters, B.J., Jiang, C., Tomsho, L.P., Qi, J., Schuster, S.C., Albert, I., and Pugh, B.F. (2008). A barrier nucleosome model for statistical positioning of nucleosomes throughout the yeast genome. Genome Res. *18*, 1073–1083.

Mieczkowski, P.A., Dominska, M., Buck, M.J., Gerton, J.L., Lieb, J.D., and Petes, T.D. (2006). Global analysis of the relationship between the binding of the Bas1p transcription factor and meiosis-specific double-strand DNA breaks in *Saccharomyces cerevisiae*. Mol. Cell. Biol. *26*, 1014–1027.

Murakami, H., and Nicolas, A. (2009). Locally, meiotic double-strand breaks targeted by Gal4BD-Spo11 occur at discrete sites with a sequence preference. Mol. Cell. Biol. *29*, 3500–3516.

Neale, M.J. (2010). PRDM9 points the zinc finger at meiotic recombination hot spots. Genome Biol. *11*, 104.

Neale, M.J., Pan, J., and Keeney, S. (2005). Endonucleolytic processing of covalent protein-linked DNA double-strand breaks. Nature *436*, 1053–1057.

Nichols, M.D., DeAngelis, K., Keck, J.L., and Berger, J.M. (1999). Structure and function of an archaeal topoisomerase VI subunit with homology to the meiotic recombination factor Spo11. EMBO J. *18*, 6177–6188.

Nicolas, A., Treco, D., Schultes, N.P., and Szostak, J.W. (1989). An initiation site for meiotic gene conversion in the yeast *Saccharomyces cerevisiae*. Nature *338*, 35–39.

Ohta, K., Shibata, T., and Nicolas, A. (1994). Changes in chromatin structure at recombination initiation sites during yeast meiosis. EMBO J. *13*, 5754–5763.

Petes, T.D. (2001). Meiotic recombination hot spots and cold spots. Nat. Rev. Genet. *2*, 360–369.

Petes, T.D., and Botstein, D. (1977). Simple Mendelian inheritance of the reiterated ribosomal DNA of yeast. Proc. Natl. Acad. Sci. USA *74*, 5091–5095.

Radman-Livaja, M., and Rando, O.J. (2010). Nucleosome positioning: how is it established, and why does it matter? Dev. Biol. *339*, 258–266.

Rockmill, B., Voelkel-Meiman, K., and Roeder, G.S. (2006). Centromere-proximal crossovers are associated with precocious separation of sister chromatids during meiosis in *Saccharomyces cerevisiae*. Genetics *174*, 1745–1754.

Sasaki, M., Lange, J., and Keeney, S. (2010). Genome destabilization by homologous recombination in the germ line. Nat. Rev. Mol. Cell Biol. *11*, 182–195.

Schlecht, U., Erb, I., Demougin, P., Robine, N., Borde, V., Nimwegen, E., Nicolas, A., and Primig, M. (2008). Genome-wide expression profiling, in vivo DNA binding analysis, and probabilistic motif prediction reveal novel Abf1 target genes during fermentation, respiration, and sporulation in yeast. Mol. Biol. Cell *19*, 2193–2207.

Tirosh, I., and Barkai, N. (2008). Two strategies for gene regulation by promoter nucleosomes. Genome Res. *18*, 1084–1091.

Tsankov, A.M., Thompson, D.A., Socha, A., Regev, A., and Rando, O.J. (2010). The role of nucleosome positioning in the evolution of gene regulation. PLoS Biol. *8*, e1000414.

Xu, F., and Petes, T.D. (1996). Fine-structure mapping of meiosis-specific double-strand DNA breaks at a recombination hot spot associated with an insertion of telomeric sequences upstream of the *HIS4* locus in yeast. Genetics *143*, 1115–1125.